An Extended Kalman Filter with Inequality Constraints for Real-time Detection of Intradialytic Hypotension

Sardar Ansari[1,*], *Member, IEEE,* Somayeh Molaei[2,*],Kenn Oldham[3,*], Michael Heung[4,*], Kevin R. Ward[5,*], Kayvan Najarian[6,*], *Senior Member, IEEE*

***Abstract*— Intradialytic hypotension (IDH) is the most common complication of hemodialysis, affecting 15-50% of all dialysis sessions. Previously, we had presented a non-invasive Polyvinylidene Fluoride (PVDF) based sensor in the form of a ring to measure vascular tone and we showed that the morphology of the signal can be utilized to predict IDH. This paper presents an approach for analyzing the PVDF signal using extended Kalman filter (EKF) and a synthetic model that has previously been used to model the ECG signal with Gaussian functions. Moreover, a novel approach for incorporating state inequality constraints into the EKF process using a gradient projection method is introduced. The taut string algorithm was first used to estimate the outline of the signal and remove it to highlight the reflection waves. Then, the EKF was used to characterize the morphology of the signal using Gaussian functions. The amplitudes of the Gaussian functions were used as features to train a classifier. The results indicated that the PPV and NPV for the prediction were 83.33% and 100%, respectively.**

***Index Terms*— Intradialytic hypotension, Polyvinylidene Fluoride, extended Kalman filter, inequality constraints, reflection waves**

I. Introduction

With more than 65 million sessions and 421,469 patients (in 2013), hemodialysis is the most common medical procedure in the US [1]. It involves extracorporeal removal of waste products from blood for patients with end-stage renal disease (ESRD). The most prevalent complication observed during hemodialysis, which affects 15 to 50% of all dialysis sessions depending on the definition, is intradialytic hypotension (IDH) [2], [3], [4]. Moreover, IDH is an abnormal drop in blood pressure (BP) during the dialysis session caused by imbalances between four variables: cardiac output, ultrafiltration rate, peripheral vascular resistance, and venoconstriction [5]. IDH has been identified as an independent risk factor for mortality, including sudden cardiac death during dialysis [6], [7]. The current standard of care for detecting IDH involves intermittent BP measurements every 5 to 15 minutes as well as subjective patient reported symptoms such as lightheadedness, weakness, muscle cramps, nausea and vomiting. Therefore, preemptive intervention to correct the trajectory of dialysis before IDH happens may have a large impact on the quality of care for ESRD patients [8]. However, IDH still remains a challenge for both patients and clinicians despite several efforts to alleviate this problem [9].

In our previous work, we introduced a novel non-invasive polyvinylidene fluoride (PVDF) based ring to monitor vascular tone [10]. This is done by measuring the displacement of arterial wall in the digital arteries. The signal that is measured by the ring is illustrated in Figure 1 which shows both the dicrotic notch and the reflection waves. The patterns of these waves are known to change in response to different physiological events such as vasoconstriction, hypotension and heart failure [11]. Therefore, we proposed an algorithm to extract features from the PVDF signal that characterize the dicrotic notch and the reflection waves. This was done by fitting five Gaussian functions to the signal, using an iterative procedure, after the outline of the signal, found by the taut string approximation algorithm [12], was removed. The parameters of Gaussian functions were used as features to train a classification model. The results indicated that changes in the patterns of the waves can be predictive of IDH. However, the iterative procedure used in [10] is time and memory intensive and is not suitable for use in portable devices with limited computational power. Moreover, the curve fitting for each period was done independently from other periods, increasing the chance of modeling noise and artifacts.

Here, we adopt a synthetic model that was originally used by McSharry et al. [13] to generate ECG signals using Gaussian functions and use it to model the reflection waves. The synthetic model is used to define the state space for an Extended Kalman Filter (EKF) that adaptively updates the parameters of the Gaussian functions. Next, a novel approach for adding inequality constraints to the Kalman Filter is introduced. The inequality constraints that are used in this paper ensure that the structure of the model is maintained throughout the process and that parameters of the model are within their normal range.

[1]Sardar Ansari is with the Department of Emergency Medicine, University of Michigan, Ann Arbor, MI, 48109 USA. e-mail: sardara@med.umich.edu.

[2]Somayeh Molaei is with the Department of Emergency Medicine, University of Michigan, Ann Arbor, MI, 48109 USA. e-mail: smolaei@med.umich.edu.

[3]Kenn Oldham is with the Department of Mechanical Engineering, University of Michigan, Ann Arbor, MI, 48109 USA. e-mail: oldham@umich.edu.

[4]Michael Heung is with the Department of Internal Medicine, University of Michigan, Ann Arbor, MI, 48109 USA. e-mail: mheung@med.umich.edu.

[5]Kevin R. Ward is with the Department of Emergency Medicine, University of Michigan, Ann Arbor, MI, 48109 USA. e-mail: keward@med.umich.edu.

[6]Kayvan Najarian is with the Department of Computational Medicine and Bioinformatics, the Department of Emergency Medicine and the Electrical Engineering and Computer Science Department, University of Michigan, Ann Arbor, MI, 48109 USA. e-mail: kayvan@med.umich.edu.

*The author is a member of the Michigan Center for Integrative Research in Clinical Care (MCIRCC), University of Michigan, Ann Arbor, MI, 48109 USA.

978-1-5090-2809-2/17/$31.00 ©2017 IEEE

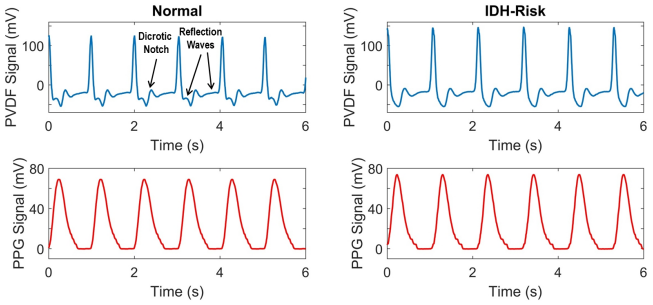

Fig. 1. A sample of the PVDF and Photoplethysmography (PPG) signals during *Normal* and *IDH-Risk* periods. The reflection waves and dicrotic notch are easily detectable in the PVDF signals. The reflection waves are diminished during the *IDH-Risk* periods. However, The PPG signal looks the same in both cases.

II. Synthetic Model and Extended Kalman Filter

In order to generate a realistic synthetic signal using a combination of Gaussian functions, Sameni et al. [14] transformed a set of 3D dynamic state equations, presented by McSharry et al. [13] into the polar form, denoted by radial coordinate z_k and angular coordinate θ_k for sample k, for the purpose of obtaining a simpler compact set, with the simplified discrete form shown as:

$$\begin{cases} \theta_k = (\theta_{k-1} + \omega\delta) \mod (2\pi) \\ z_k = -\sum_{i=1}^{N} \delta \frac{\alpha_i \omega}{\sigma_i^2} \Delta\gamma_i \exp(-\frac{\Delta\gamma_i^2}{2\sigma_i^2}) + z_{k-1} + \eta \end{cases} \quad (1)$$

where α_i, σ_i, γ_i are the amplitude, angular spread, and location of the Gaussian functions, N is the number of Gaussian functions, $\Delta\gamma_i = (\theta_k - \gamma_i) \mod (2\pi)$ is the angular distance to the center of the i^{th} Gaussian function, δ is the sampling time, ω is the angular speed and η is random white noise modeling the baseline wander and other types of additive noise. The signal can be generated by a sequence of discrete samples calculated using z. The angular speed is set to $\omega = \frac{2\pi}{l\delta}$ where l is the number of samples in the current beat. This guarantees that θ_k varies from 0 to 2π within a beat. This also ensures that the Gaussian approximation of the signal remains continuous at the beat boundaries (i.e., at 0 and 2π). It is assumed that the Gaussian parameters vary slowly with time. Therefore, their behavior can be modeled using an autoregressive (AR) dynamic models as proposed in [15]:

$$p_i(k) = p_i(k-1) + u_i(k) \quad (2)$$

where p_i denotes any of the $3N$ Gaussian parameters α_i, σ_i and γ_i while u_i indicates the corresponding white noise. For constructing the EKF structure, we use the state vector and process noise vector as introduced in [15],

$$\mathbf{x}_k = [\theta_k, z_k, \alpha_1, \ldots, \alpha_N, \sigma_1, \ldots, \sigma_N, \gamma_1, \ldots, \gamma_N]^T \quad (3)$$

$$\mathbf{y}_k = [\theta_k, z_k]^T \quad (4)$$

$$\mathbf{w}_k = [\omega, \eta, u_1, \ldots, u_{15}]^T \quad (5)$$

The extended Kalman filter (EKF) is developed for cases where the state and observation functions, $f(\cdot)$ and $h(\cdot)$, are nonlinear. The nonlinear state and observation equations can be linearized using first order Taylor series:

$$\begin{aligned} \mathbf{x}_k &= f(\mathbf{x}_{k-1}) + \mathbf{w}_k \approx \\ & f(\hat{\mathbf{x}}_{k-1}) + \mathbf{A}_{k-1}(\mathbf{x}_{k-1} - \hat{\mathbf{x}}_{k-1}) + \mathbf{w}_k \end{aligned} \quad (6)$$

$$\begin{aligned} \mathbf{y}_k &= h(\mathbf{x}_k) + \mathbf{v}_k \approx \\ & h(\hat{\mathbf{x}}_k) + \mathbf{H}_k(\mathbf{x}_k - \hat{\mathbf{x}}_k) + \mathbf{v}_k \end{aligned} \quad (7)$$

where $f(\cdot)$ is a known nonlinear model representing the dynamics of the state transition from $\mathbf{x}_{k-1}$ to $\mathbf{x}_k$ and $h(\cdot)$ is a known nonlinear model representing the transformation from the state variables to the observation $\mathbf{y}_k$ and

$$\mathbf{A}_k = \frac{\partial f(\mathbf{x})}{\partial \mathbf{x}} \mid_{\mathbf{x}=\hat{\mathbf{x}}_k} \quad (8)$$

$$\mathbf{H}_k = \frac{\partial h(\mathbf{x})}{\partial \mathbf{x}} \mid_{\mathbf{x}=\hat{\mathbf{x}}_k} . \quad (9)$$

Here, $\mathbf{w}_k$ and $\mathbf{v}_k$ are the process and measurement noises, with covariance matrices $\mathbf{Q}_k = E\{\mathbf{w}_k \mathbf{w}_k^T\}$ and $\mathbf{R}_k = E\{\mathbf{v}_k \mathbf{v}_k^T\}$, respectively. The process of the EKF can be summarized in the following as

$$\begin{cases} \hat{\mathbf{x}}_{k|k-1} = f(\hat{\mathbf{x}}_{k-1|k-1}) \\ \mathbf{P}_{k|k-1} = \mathbf{A}_{k-1}\mathbf{P}_{k-1|k-1}\mathbf{A}_{k-1}^T + \mathbf{Q}_k \end{cases} \quad (10)$$

$$\begin{cases} \mathbf{K}_k = \mathbf{P}_{k|k-1}\mathbf{H}_k^T[\mathbf{H}_k\mathbf{P}_{k|k-1}\mathbf{H}_k^T + \mathbf{R}_k]^{-1} \\ \hat{\mathbf{x}}_{k|k} = \hat{\mathbf{x}}_{k|k-1} + \mathbf{K}_k[\mathbf{y}_k - h(\hat{\mathbf{x}}_{k|k-1})] \\ \mathbf{P}_{k|k} = (\mathbf{I} - \mathbf{K}_k\mathbf{H}_k)\mathbf{P}_{k|k-1} \end{cases} \quad (11)$$

where $\hat{\mathbf{x}}_{k|k-1} = E\{\mathbf{x}_k|\mathbf{y}_{k-1}, \mathbf{y}_{y-2}, \ldots, \mathbf{y}_1\}$ is the least square error *a prior* estimate of the state vector at the k^{th} update, using the prior observations $\mathbf{y}_1$ to $\mathbf{y}_{k-1}$, and $\hat{\mathbf{x}}_{k|k} = E\{\mathbf{x}_k|\mathbf{y}_k, \mathbf{y}_{k-1}, \mathbf{y}_{k-2}, \ldots, \mathbf{y}_1\}$ is the *a posteriori* estimate of the state vector after adding the *k*th observations $\mathbf{y}_k$. $\mathbf{P}_{k|k-1}$ and $\mathbf{P}_{k|k}$ are defined in the same manner to be the estimations of covariance matrices for the state approximation errors in the *k*th stage before and after using the *k*th observation, respectively. The equations for the derivatives of f with respect to $\mathbf{x}$, which define matrix $\mathbf{A}$, can be found in [15].

III. Extended Kalman Filter with State Inequality Constraints

Kalman filter's state transitions can lead to infeasible or undesirable states. Such states can be avoided by adding constraints to the Kalman filter. The Kalman filter with equality constraints has a closed-form solution that can be found efficiently [16]. However, the solution for a Kalman filter with inequality constraints cannot be expressed in closed-form and must be derived numerically [17]. Here, we use a projection method [18] that projects the vector of state update onto the constraint surface to ensure that the updated state variable is always feasible. This can result in a suboptimal solutions; however, the numerous updates that are performed within each period of the signal would allow the

EKF to track the optimal solution while avoiding infeasible solutions.

The linear constraints on the state variable $\mathbf{x}_{k|k}$ can be expressed as

$$\mathbf{z} = \mathbf{C}\mathbf{x}_{k|k} - \mathbf{d} \geq \mathbf{0} \tag{12}$$

Moreover, the update equation in (11) can be written as

$$\hat{\mathbf{x}}_{k|k} = \hat{\mathbf{x}}_{k|k-1} + \mathbf{u}_k \tag{13}$$

where $\mathbf{u}_k = \mathbf{K}_k \boldsymbol{v}_k$ is the update vector and $\boldsymbol{v}_k$ is the innovation signal defined as $\boldsymbol{v}_k = [\mathbf{y}_k - h(\hat{\mathbf{x}}_{k|k-1})]$. The state vector after projection, $\hat{\mathbf{x}}^p_{k|k}$, can be obtained by projecting the update vector using a projection matrix $\mathbf{B}$ as follows

$$\hat{\mathbf{x}}^p_{k|k} = \hat{\mathbf{x}}_{k|k-1} + \mathbf{B}\mathbf{u}_k. \tag{14}$$

We form a matrix $\mathbf{N}$ whose columns are the gradients of active constraints (i.e., holding at equality) for which the update vector points towards their infeasible region, i.e., $(\mathbf{C}^{i,\cdot})^{\mathrm{T}}\mathbf{u}_k \leq 0$ where $\mathbf{C}^{i,\cdot}$ is the i^{th} row of $\mathbf{C}$. Then, the projection matrix $\mathbf{B}$ can be found as

$$\mathbf{B} = \alpha\mathbf{D} = \alpha(\mathbf{I} - \mathbf{N}(\mathbf{N}^T\mathbf{N})^{-1}\mathbf{N}). \tag{15}$$

The variable α ensures that the update does not violate any inactive constrains and is found by

$$\alpha = \min\left(\frac{-(\mathbf{C}^{i,\cdot})^{\mathrm{T}}\hat{\mathbf{x}}_{k|k-1} + \mathbf{d}^i}{(\mathbf{C}^{i,\cdot})^{\mathrm{T}}\mathbf{D}\mathbf{u}_k}, 1\right) \tag{16}$$

for $\{i|(\mathbf{C}^{i,\cdot})^{\mathrm{T}}\mathbf{D}\mathbf{u}_k < 0\}$. Note that $\mathbf{d}^i$ is the i^{th} element of vector $\mathbf{d}$.

Next, we need to find the covariance matrix for the error of *a posteriori* state approximation after projection, $\mathbf{P}^p_{k|k}$. The state approximation error can be expressed as

$$\tilde{\mathbf{x}}^p_{k|k} = \tilde{\mathbf{x}}_{k|k-1} - \mathbf{B}\mathbf{u}_k \tag{17}$$

where $\tilde{\mathbf{x}}^p_{k|k} = \mathbf{x}_k - \hat{\mathbf{x}}^p_{k|k}$ and $\tilde{\mathbf{x}}_{k|k-1} = \mathbf{x}_k - \hat{\mathbf{x}}_{k|k-1}$. Hence, $\mathbf{P}^p_{k|k}$ can be derived as

$$\begin{aligned}
&\mathbf{P}^p_{k|k} = E[\tilde{\mathbf{x}}^p_{k|k}(\tilde{\mathbf{x}}^p_{k|k})^{\mathrm{T}}] = \\
&E[(\tilde{\mathbf{x}}_{k|k-1} - \mathbf{B}\mathbf{u}_k)(\tilde{\mathbf{x}}_{k|k-1} - \mathbf{B}\mathbf{u}_k)^{\mathrm{T}}] = \\
&\mathbf{P}_{k|k-1} - E[\tilde{\mathbf{x}}_{k|k-1}\boldsymbol{v}_k^{\mathrm{T}}]\mathbf{K}_k^{\mathrm{T}}\mathbf{B}^{\mathrm{T}} + \\
&\mathbf{B}\mathbf{K}_k E[\boldsymbol{v}_k\boldsymbol{v}_k^{\mathrm{T}}]\mathbf{K}_k^{\mathrm{T}}\mathbf{B}^{\mathrm{T}} - \mathbf{B}\mathbf{K}_k E[\boldsymbol{v}_k\tilde{\mathbf{x}}_{k|k-1}^{\mathrm{T}}].
\end{aligned} \tag{18}$$

Given that $\mathbf{K}_k E[\boldsymbol{v}_k\boldsymbol{v}_k^{\mathrm{T}}] = \mathbf{P}_{k|k-1}\mathbf{H}_k^{\mathrm{T}}$ and $E[\tilde{\mathbf{x}}_{k|k-1}\boldsymbol{v}_k^{\mathrm{T}}] = \mathbf{P}_{k|k-1}\mathbf{H}_k^{\mathrm{T}}$, one can derive the equation for $\mathbf{P}^p_{k|k}$ as

$$\mathbf{P}^p_{k|k} = \mathbf{P}_{k|k-1} - \mathbf{G}\mathbf{B} - \mathbf{B}^{\mathrm{T}}\mathbf{G}^{\mathrm{T}} + \mathbf{B}\mathbf{G}\mathbf{B}^{\mathrm{T}} \tag{19}$$

where $\mathbf{G} = \mathbf{P}_{k|k-1}\mathbf{H}^{\mathrm{T}}\mathbf{K}_k^{\mathrm{T}}$.

IV. Data Collection

The data collection was done during dialysis sessions at the inpatient acute dialysis unit at University of Michigan. The signals were collected using a Biopac MP150 equipped with DA100C, BN-PPGED, BN-RSPEC and BN-ACCL3 modules to acquire the PVDF, photoplethysmography (PPG), electrocardiogram (ECG) and accelerometer signals, respectively. The PVDF signal was low-pass filtered at 10Hz and amplified with a gain of 50. The ring was placed on the non-access hand, except for one subject whose non-access arm was broken. A total of 12 subjects participated in the study, five of them experienced IDH.

The signals were labeled as *IDH-Risk* if systolic BP (SBP)<100mmHg when predialysis SBP<160mmHg or SBP<110mmHg when predialysis SBP≥160mmHg. This is a relaxed (by 10mmHg) version of the definition offered in [7] to account for the compensation period prior to IDH. One patient had a baseline SBP of 92mmHg for whom the signal was marked as *IDH-Risk* when SBP dropped by 10mmHg.

V. Signal Analysis

The collected signals were preprocessed using a process similar to the one presented in [10]. The heart beats were detected using the ECG and PPG signals and the PVDF periods were averaged to remove motion artifacts and other noise in the signal. Then, the beat detection was performed on the averaged signal to find the R waves (peaks that correspond to the heart beat). The envelope of the signal was used to scale the signal between zero and one. The averaged signal and its envelope are shown in Figure 2a. Next, the taut string approximation algorithm with an $\varepsilon = 0.05$ was used to estimate the outline of the normalized PVDF signal, depicted in Figure 2b. Therefore, the residual signal is guaranteed to have an amplitude of less than 0.05. The residual signal highlights the reflection waves and the dicrotic notch which can be hard to model due to their small amplitude relative to the amplitude of the main peak. Moreover, the residual signal, after adding ε, would have a baseline of zero making it easy to model the signal with Gaussian functions.

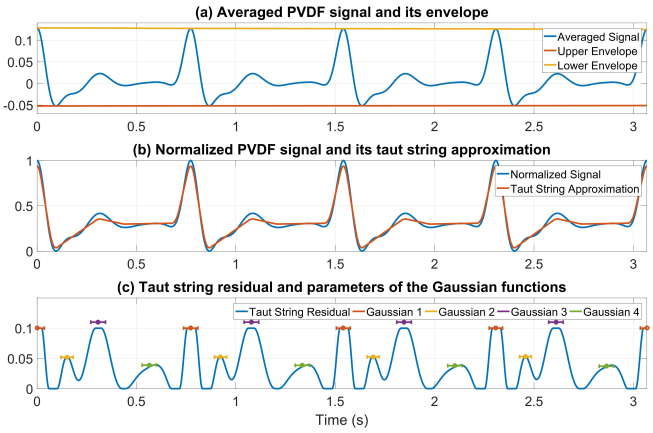

Fig. 2. The results of different steps of signal analysis including (a) period averaging, (b) normalizing and finding the outline and (c) applying constrained EKF to the residuals. The markers in (c) indicate the location and amplitude of the Gaussian functions as well as the spread of the function with the horizontal error bars.

The EKF with inequality constraints described in Sections II and III was used to model the residual signal. Four Gaussian functions were used to model the main beat, dicrotic notch and two reflection waves ($N = 4$). Three types of constraints were applied to state variables. First, the amplitude of the Gaussian functions should be positive, i.e.,

$\alpha_i \geq 0, \forall i \in [1, N]$. The second set of constraints ensured that the spreads of Gaussian functions are within a reasonable range, i.e., $0.01 \leq \sigma_i \leq 0.3, \forall i \in [1, N]$. Finally, a set of constraints were used to ensure that the Gaussian functions do not overlap, expressed as $2\pi + \gamma_1 - \gamma_N \geq 2(\sigma_1 + \sigma_N)$ and $\gamma_i - \gamma_{i-1} \geq 2(\sigma_i + \sigma_{i-1}), \forall i \in [2, N]$. The amplitude of the residual signal at the center of the four Gaussian functions, γ_i, were used as features to train a classification model that separates the *Normal* and *IDH-Risk* periods of the signals. The covariance matrices $\mathbf{Q}$ and $\mathbf{R}$ were manually designed based on the domain knowledge regarding the rate of change for each of the parameters. The same matrices were used to process all the subjects.

VI. Results

The signals were sampled every minute creating a total of 2325 instances. For the positive subjects that experienced IDH, only the *IDH-Risk* section of the signal prior to the IDH event was used, resulting in 232 positive instances. The same number of negative instances were randomly selected from the negative subjects. This resulted in a feature set that included 4 features and 446 instances from five positive and seven negative subjects for classification. After standardizing the data, Support vector machines (SVM) classification models with linear and RBF kernels were trained to classify the *Normal* and *IDH-Risk* instances. The training and testing of the models were done using nested cross-validation (CV) to ensure generalizability of the results. In each iteration, one of the subjects was held out for testing and the remaining subjects were used for training with cross-validation. Grid search was performed in the inner loop to find the best C parameter and σ for the RBF kernel. The trained SVM model using the best parameters was applied the testing subject's full signal.

An alarm was declared only if the signal was continuously classified as *IDH-Risk* for two minutes. An IDH event was correctly predicted if the alarm was raised prior to the incident. On the other hand, when the signal was continuously classified as *IDH-Risk* for two minutes for a negative subject, a false alarm was recorded. All of the five positive subjects had their IDH episodes predicted correctly and the mean and median prediction times were 88 and 101 minutes, respectively. For six negative subjects, the alarm was not raised while a false alarm was reported for one of the negative subjects. Therefore, the positive predictive value and negative predictive values were 83.33% and 100%, respectively. This shows that the combination of the PVDF sensor and the proposed approach for analyzing its signal can be used effectively to predict and eventually avert the risk of IDH.

VII. Conclusions

A novel approach for analyzing the signal that is obtained from a previously introduced Polyvinylidene Fluoride based non-invasive sensor to predict IDH has been proposed in this paper. The approach utilizes EKF with state inequality constraints and a synthetic model of Gaussian functions to characterize the reflection waves in the signal. The data was collected from dialysis patients to assess the performance of the proposed method for predicting IDH. The results indicate that the PVDF signal along with the analytical approach that is presented in this paper can be used to predict IDH.

References

[1] U. S. R. D. System, "2015 USRDS annual data report: Epidemiology of kidney disease in the united states," National Institutes of Health, National Institute of Diabetes and Digestive and Kidney Diseases, Bethesda, MD, Tech. Rep., 2015.

[2] B. F. Palmer and W. L. Henrich, "Recent advances in the prevention and management of intradialytic hypotension," *Journal of the American Society of Nephrology*, vol. 19, no. 1, pp. 8–11, 2008.

[3] J. J. Sands, L. A. Usvyat, T. Sullivan, J. H. Segal, P. Zabetakis, P. Kotanko, F. W. Maddux, and J. A. Diaz-Buxo, "Intradialytic hypotension: frequency, sources of variation and correlation with clinical outcome," *Hemodialysis International*, vol. 18, no. 2, pp. 415–422, 2014.

[4] W. Bradshaw *et al.*, "Intradialytic hypotension: a literature review," *Renal Society of Australasia Journal*, vol. 10, no. 1, p. 22, 2014.

[5] C. Barth, W. Boer, D. Garzoni, T. Kuenzi, W. Ries, R. Schaefer, D. Schneditz, T. Tsobanelis, F. van der Sande, R. Wojke, *et al.*, "Characteristics of hypotension-prone haemodialysis patients: is there a critical relative blood volume?" *Nephrology Dialysis Transplantation*, vol. 18, no. 7, pp. 1353–1360, 2003.

[6] B. V. Stefánsson, S. M. Brunelli, C. Cabrera, D. Rosenbaum, E. Anum, K. Ramakrishnan, D. E. Jensen, and N.-O. Stålhammar, "Intradialytic hypotension and risk of cardiovascular disease," *Clinical Journal of the American Society of Nephrology*, vol. 9, no. 12, pp. 2124–2132, 2014.

[7] J. E. Flythe, H. Xue, K. E. Lynch, G. C. Curhan, and S. M. Brunelli, "Association of mortality risk with various definitions of intradialytic hypotension," *Journal of the American Society of Nephrology*, pp. ASN–2 014 020 222, 2014.

[8] J. T. Daugirdas, "Measuring intradialytic hypotension to improve quality of care," *Journal of the American Society of Nephrology*, vol. 26, no. 3, pp. 512–514, 2015.

[9] W. Bradshaw and P. N. Bennett, "Asymptomatic intradialytic hypotension: the need for pre-emptive intervention," *Nephrology Nursing Journal*, vol. 42, no. 5, p. 479, 2015.

[10] S. Ansari, N. Farzaneh, M. Heung, K. Oldham, H. Derksen, K. R. Ward, and K. Najarian, "Real-time detection of intradialytic hypotension using a novel polyvinylidene fluoride based sensor," in *2016 IEEE-EMBS International Conference on Biomedical and Health Informatics (BHI)*. IEEE, 2016, pp. 493–496.

[11] W. Grossman and D. S. Baim, *Grossman's cardiac catheterization, angiography, and intervention*. Lippincott Williams & Wilkins, 2006.

[12] R. Barlow, *Statistical inference under order restrictions; the theory and application of isotonic regression*. Wiley New York, 1972.

[13] P. E. McSharry, G. D. Clifford, L. Tarassenko, and L. A. Smith, "A dynamical model for generating synthetic electrocardiogram signals," *IEEE Transactions on Biomedical Engineering*, vol. 50, no. 3, pp. 289–294, 2003.

[14] R. Sameni, M. Shamsollahi, C. Jutten, and M. Babaie-Zade, "Filtering noisy ECG signals using the extended kalman filter based on a modified dynamic ECG model," in *Computers in Cardiology, 2005*. IEEE, 2005, pp. 1017–1020.

[15] O. Sayadi and M. B. Shamsollahi, "ECG denoising and compression using a modified extended kalman filter structure," *IEEE Transactions on Biomedical Engineering*, vol. 55, no. 9, pp. 2240–2248, 2008.

[16] N. Gupta and R. Hauser, "Kalman filtering with equality and inequality state constraints," *arXiv preprint arXiv:0709.2791*, 2007.

[17] D. Simon, "Kalman filtering with state constraints: a survey of linear and nonlinear algorithms," *IET Control Theory & Applications*, vol. 4, no. 8, pp. 1303–1318, 2010.

[18] J. B. Rosen, "The gradient projection method for nonlinear programming. part i. linear constraints," *Journal of the Society for Industrial and Applied Mathematics*, vol. 8, no. 1, pp. 181–217, 1960.